Applied Thermal Engineering 79 (2015) 192–201

Contents lists available at ScienceDirect

Applied Thermal Engineering

journal homepage: www.elsevier.com/locate/apthermeng

Research paper

A generalized moving-boundary algorithm to predict the heat transfer rate of counterflow heat exchangers for any phase configuration

Ian H. Bell [a, *], Sylvain Quoilin [a], Emeline Georges [a], James E. Braun [b], Eckhard A. Groll [b], W. Travis Horton [b], Vincent Lemort [a]

[a] University of Liège, Energy Systems Research Unit, Liège, Belgium
[b] Purdue University, Department of Mechanical Engineering, 140 S. Martin Jischke Drive, West Lafayette, IN 47906, USA

HIGHLIGHTS

- Generalized method presented to predict heat transfer rate of heat exchangers for all phase configurations.
- Considers both internal and external pinching in the heat exchanger.
- Bounded solver used for excellent robustness of the solution.
- Source code for the method is presented in the python programming language.

ARTICLE INFO

Article history:
Received 19 May 2014
Accepted 14 December 2014
Available online 23 December 2014

Keywords:
Heat exchangers
Simulation
Moving boundary

ABSTRACT

In this work, a novel and robust solution approach is presented that can be used to predict the steady-state thermal heat transfer rate for counterflow heat exchangers with any combination of single-phase and two-phase conditions within the heat exchanger. This methodology allows for multiple internal pinching points, as well as all permutations of subcooled liquid, two-phase and superheated vapor sections for the hot and cold fluids. A residual function based on the matching of the required and available thermal conductances in each section is derived, and Brent's method is then used to drive the residual to zero. Examples are presented for the application of this methodology to a water-heated n-Propane evaporator. The computational time required to execute the model for a simple case is on the order of one millisecond when the tabular interpolation methods of CoolProp are applied. Source code for the algorithm is provided in the Python programming language as an appendix.

1. Introduction

Counterflow heat exchangers are found throughout engineered thermal systems, including air-conditioning, refrigeration, small-scale energy generation, food processing and chemical industries. They are often found in the form of brazed plate heat exchangers or coaxial tube-in-tube heat exchangers.

Heat exchangers are often part of multi-component systems, and their accurate modeling is of major importance for performance assessment and control purposes. In the last fifty years, several studies have focused on the determination of the fluid temperature distribution along the heat exchanger. One of the first works was carried out by Wolf [15] and focused on the resolution of equations for parallel-flow multichannel heat exchangers for stationary heat exchange processes. General systems of first order differential equations were derived and solved by matrix manipulations. The solution obtained was expressed as a linear combination of exponential functions.

1.1. General heat exchanger analysis

Settari and Venart [13] developed a method to approximate the exact analytical solution based on a polynomial approximation of the temperature profiles in each channel of the heat exchanger. Their method was found to give good results only for a specific range of NTU (Number of Transfer Units) values and number of

* Corresponding author.
E-mail addresses: ian.bell@ulg.ac.be (I.H. Bell), squoilin@ulg.ac.be (S. Quoilin), emeline.georges@ulg.ac.be (E. Georges), jbraun@purdue.edu (J.E. Braun), groll@purdue.edu (E.A. Groll), wthorton@purdue.edu (W.T. Horton), vincent.lemort@ulg.ac.be (V. Lemort).

http://dx.doi.org/10.1016/j.applthermaleng.2014.12.028
1359-4311/

Nomenclature

A_c	area on cold side (m^2)
A_h	area on hot side (m^2)
$\overrightarrow{h}_c$	enthalpy vector of cold stream (J kg^{-1} K^{-1})
$\overrightarrow{h}_h$	enthalpy vector of hot stream (J kg^{-1} K^{-1})
$\widehat{h}$	normalized enthalpy parameter
$h_{c,bub}$	cold stream bubble point enthalpy (J kg^{-1} K^{-1})
$h_{c,dew}$	cold stream dew point enthalpy (J kg^{-1} K^{-1})
$h_{c,i}$	cold stream inlet enthalpy (J kg^{-1} K^{-1})
$h_{c,o}$	cold stream outlet enthalpy (J kg^{-1} K^{-1})
$h_{c,pinch}$	cold stream pinch enthalpy (J kg^{-1} K^{-1})
$h_{h,bub}$	hot stream bubble point enthalpy (J kg^{-1} K^{-1})
$h_{h,dew}$	hot stream dew point enthalpy (J kg^{-1} K^{-1})
$h_{h,i}$	hot stream inlet enthalpy (J kg^{-1} K^{-1})
$h_{h,o}$	hot stream outlet enthalpy (J kg^{-1} K^{-1})
$h_{h,pinch}$	hot stream pinch enthalpy (J kg^{-1} K^{-1})
LMTD	log-mean-temperature-difference (K)
$\dot{m}_c$	cold stream mass flow rate (kg s^{-1})
$\dot{m}_h$	hot stream mass flow rate (kg s^{-1})
$p_{c,i}$	cold stream inlet pressure (Pa)
$p_{h,i}$	hot stream inlet pressure (Pa)
ΔT_A	temperature difference A (K)
ΔT_B	temperature difference B (K)
$\overrightarrow{T}_c$	temperature vector of cold stream (K)
$\overrightarrow{T}_h$	temperature vector of hot stream (K)
$T_{c,i}$	cold stream inlet temperature (K)
$T_{c,o}$	cold stream outlet temperature (K)
$T_{h,i}$	hot stream inlet temperature (K)
$T_{h,o}$	hot stream outlet temperature (K)
$\dot{Q}$	heat transfer rate (W)
$\dot{Q}_{cell}$	cell heat transfer rate (W)
$\dot{Q}_k$	heat transfer rate in cell (W)
$\dot{Q}_{\max,ext}$	external pinching heat transfer rate (W)
$\dot{Q}_{\max,int}$	internal pinching heat transfer rate (W)
$\dot{Q}_{h,max}$	hot stream max heat transfer (W)
$\dot{Q}_{c,max}$	cold stream max heat transfer (W)
R_{cond}	conduction resistance based on A_h (K W^{-1})
UA_{avail}	available conductance (W K^{-1})
UA_{req}	required conductance (W K^{-1})
w_k	area fraction for cell
α_c	cold stream heat transfer coefficient (W m^{-2} K^{-1})
α_h	hot stream heat transfer coefficient (W m^{-2} K^{-1})

channels. Zaleski and Keplacka [17] then suggested to use exponential functions instead of polynomials and could extend the range of NTUs for which the method gave excellent approximations. Their results were in accordance with those obtained by Kandlikar and Shah [6] who solved the finite difference equations using the Gauss–Seidel iterative method. In 2002, Ribeiro and Andrade [12], developed an algorithm to use with the combination of exponential functions as explored by Zaleski and Keplacka that can handle any flow patterns, and is based on the knowledge or iterative calculation of an overall heat transfer coefficient for the heat exchanger.

1.2. Finite volume and moving boundary models

More recently, different studies have been carried out on both steady-state and dynamic modeling of heat exchangers. Amongst the proposed models, one [4] distinguishes moving-boundary (or lumped parameters) and finite volume methods. Qiao et al. [10] developed a finite volume steady-state model of plate heat exchangers for any flow configurations including phase-change on both sides and flow maldistribution. Parallel solving for the different elements was investigated.

Solving moving-boundary models is a non-linear implicit problem that can lead to convergence issues if proper guess variables are not provided. The issue of inadequate guess values is well known by all users of such models and significantly decreases the robustness of the proposed models. However, very few solutions are proposed in the literature to address this problem.

The most common algorithm to solve non-linear systems of equations is the Newton Solver. The efficiency of the solving process can however vary depending on how the system of equations is expressed. In a causal formulation, each equation can be solved explicitly and the solution algorithm iterates on this set of explicit equations. In an acausal formulation, the solver selects state variables and uses the Newton Method to minimize a vector of residual functions. When integrated into a more general model, the state variables of the heat exchanger models are solved simultaneously with the state variables of the outer models.

Simulation issues generally arise when the iteration process leads the Newton solver to evaluate a physically-impossible solution (typically crossing of the temperature profiles). This can be due to the heat exchanger model itself, or to the outer models imposing impossible operating conditions to the heat exchanger. In that case, the computation of the heat transfer is not possible and leads to numerical issues such as logarithms of negative numbers in the LMTD method.

To avoid this situation, proper guess values to start the iteration process are required. However, this is time consuming and requires experienced end-users. A solution was proposed by Quoilin [11] using a numerical artifact for the computation of the heat transfer: in that approach, the model is expressed in a causal way, with the inlet/outlet conditions of each fluid as input and the required heat exchanger area as output. The solver then iterates on the inlet/outlet conditions to obtain the proper (imposed) heat exchanger area. To deal with physically-impossible operating conditions, the LMTD equations were modified to allow negative temperature differences. In that case a high penalty is imposed to the output heat exchange area, which drives the solver out of the physically-impossible zone.

It should also be noted that most of the moving-boundary models in the literature are designed for particular cases, such as liquid on the hot side and two-phase and vapor on the cold side (case of a refrigeration evaporator). These models cannot readily be used in other situations (e.g. as a condenser).

1.3. Overview

In this paper an algorithm is proposed that solves the two issues described above:

- It is designed to handle any combination/arrangement of fluid states on both sides.
- It is designed in such a way that the iteration process cannot lead to physically-impossible temperature profiles.

According to Bendapudi et al. [2]; moving boundary models are up to three times faster than finite volume approaches, hence very

useful for "real time" simulations. The solution technique proposed here allows one model to solve for the full range of possible steady state operating conditions in the heat exchanger. This includes the most complex case involving phase-change in both fluids. A general pinch point analysis is carried out, based on a principle similar to the work of Yohanis et al. [16]; who presented a method of determination of the maximum heat transfer rate with minimum information on the heat exchanger characteristics. In this work, special attention is also paid to the solution method.

2. Methodology

The heat exchangers under study in this paper are counterflow heat exchangers, which have two streams (hot and cold) separated by a wall, although this method can be readily extended to cross-flow or cross-counterflow heat exchangers. Knowing the inlet states of both streams and the dimensions of the heat exchanger, the amount of heat transferred by the hot stream to the cold stream is calculated. At all locations in the heat exchanger, the hot stream must be hotter than the cold stream.

This algorithm is summarized in Fig. 1. The steps are:

1. Determine the maximum possible heat transfer rate based on the assumption of external pinching (based only on inlet and outlet states of the heat exchanger) at the outlet of the limiting stream, as seen in Fig. 2(a).
2. Decrease the maximum possible heat transfer rate due to internal pinch points (based on phase transitions that occur inside the heat exchanger) if any are present, as seen in Fig. 2(b)
3. Obtain iteratively the actual heat transfer rate of the heat exchanger using a bounded numerical solver employing the physical bounds for the heat transfer rate, as seen in Fig. 2(c).

The enabling insight of this model solution approach is that if the mass flow rates of each stream, the inlet enthalpies of each stream, and the total heat transfer rate are known, it is possible to divide the heat exchanger into a number of cells, where in each cell the phase (liquid, vapor, two-phase) of each fluid is the same throughout the entire cell. Here, a phase boundary is defined as a location where one stream changes between a single-phase (subcooled liquid or superheated vapor) and a two-phase state, or vice versa.

Fig. 2 shows the algorithm in temperature profile versus normalized enthalpy form. In the first step (Fig. 2(a)), the external pinch point analysis is applied, which predicts an external pinch point at the outlet of the hot stream/inlet of the cold stream. It is important to note that the hot stream temperature is lower than the cold stream temperature in the central part of the heat exchanger which is a physically-impossible configuration. In the second step (Fig. 2(b)), the internal pinching analysis is applied which yields an internal pinching point in the heat exchanger. Finally the full solution (Fig. 2(c)) is carried out based on the bounding value for the heat transfer rate from the internal pinching. The detailed analysis required for each part of this solution approach will be covered in the following sections. The parameter $\widehat{h}$ is a normalized enthalpy value, which is given by

$$\widehat{h} = \frac{\dot{m}\left(\overrightarrow{h} - \min\left(\overrightarrow{h}\right)\right)}{\dot{Q}} \tag{1}$$

for both the hot and cold streams.

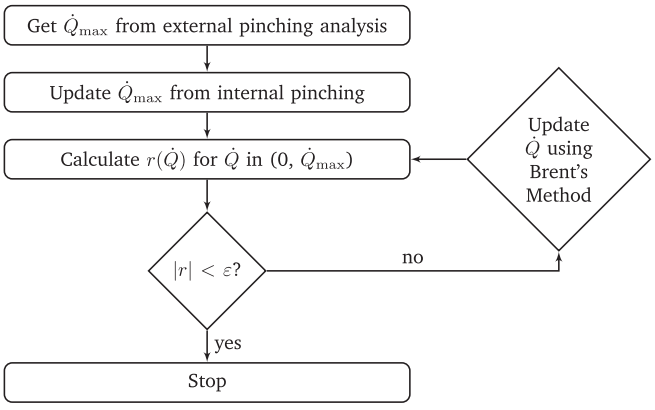

Fig. 1. Flow chart for heat exchanger algorithm.

2.1. Model limitations

Due to the formulation of this model, it is not possible to consider the effects of pressure drop on enthalpy and two-phase temperature glide. The assumption of no pressure drop tends to be a good assumption for brazed plate heat exchangers (which are typically designed for a low pressure drop). For other styles of heat exchanger, the assumption of no pressure drop can be a less suitable assumption.

Furthermore, a second limitation is that the pressures of the fluids must be sub-critical. This limitation is required to ensure that the thermophysical properties of the fluids in each part of the heat exchanger can be fairly treated as being constant. Most importantly, this limitation is required to avoid the pseudo-critical spike in the viscosity and thermal conductivity for supercritical conditions.

2.2. Thermophysical properties

The thermodynamic and transport properties of the working fluids are obtained through the use of CoolProp, a reference-grade, open-source thermophysical property library [1]. This library implements the most accurate equations of state available in the literature, as well as highly efficient tabular interpolation methods, incompressible fluids and brines. Furthermore, CoolProp can be used as an interface layer around REFPROP [7] in most programming environments of practical interest.

2.3. External pinching

The second law of thermodynamics states that heat can only be transferred from higher temperature to lower temperature. As a consequence of this law, it is possible to obtain a preliminary estimate for the heat transferred within a counterflow heat exchanger. The second law of thermodynamics imposes the following limits on the outlet states of each stream:

- The outlet temperature of the cold stream must be less than or equal to the inlet temperature of the hot stream
- The outlet temperature of the hot stream must be greater than or equal to the inlet temperature of the cold stream

These conditions can also be expressed algebraically as:

$$T_{h,o} \geq T_{c,i} \tag{2}$$

$$T_{c,o} \leq T_{h,i} \tag{3}$$

These conditions can be applied for any combination of single-phase and two-phase inlet and outlet states.

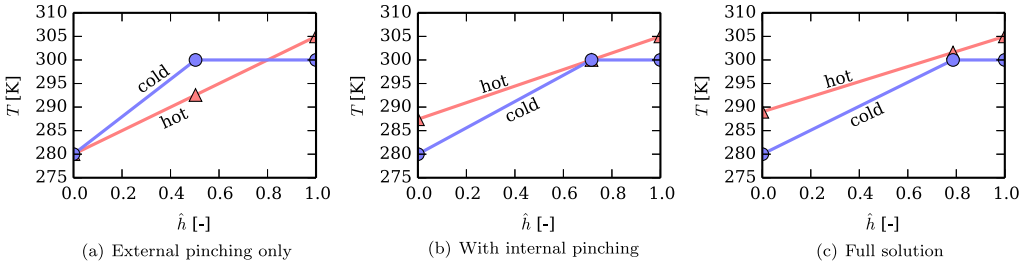

Fig. 2. Graphical representation of flow chart for water-heated n-Propane evaporator of Table 3.

The limiting temperatures of each fluid are calculated using the above analysis; it is then possible to calculate the maximum possible heat transfer rate. The upper bound for the heat transfer rate is obtained as the minimum of the heat transfer rates calculated by taking each stream to its limiting outlet state (where the outlet temperature is equal to the inlet temperature of the other stream).

The maximum heat transfer rate of the hot stream is calculated from

$$\dot{Q}_{h,\max} = \dot{m}_h(h_{h,i} - h_{h,o}) \tag{4}$$

where the outlet enthalpy of the hot stream ($h_{h,o}$) is calculated from the inlet pressure of the hot stream and the inlet temperature of the cold stream. Or expressed alternatively

$$h_{h,o} = h\left(T_{c,i}, p_{h,i}, \text{Fluid}_h\right). \tag{5}$$

Similarly, the maximum heat transfer rate of the cold stream can be obtained from

$$\dot{Q}_{c,\max} = \dot{m}_c(h_{c,o} - h_{c,i}) \tag{6}$$

where the limiting outlet enthalpy of the cold stream can be obtained from

$$h_{c,o} = h\left(T_{h,i}, p_{c,i}, \text{Fluid}_c\right). \tag{7}$$

Finally the maximum heat transfer rate given by the external pinching can be obtained from

$$\dot{Q}_{\max,ext} = \min\left(\dot{Q}_{h,\max}, \dot{Q}_{c,\max}\right). \tag{8}$$

2.4. Internal pinching

The external pinching analysis carried out in the previous step is based on the inlet and outlet states of the heat exchanger. This external pinching analysis does not consider the temperature profiles inside the heat exchanger. It is possible that the temperature profiles of the hot and cold fluid cross in the interior of the heat exchanger, which indicates a physically-impossible temperature profile caused by the external pinching analysis yielding a bound for the heat transfer rate that is too large. In order to obtain hot and cold fluid temperature profiles that do not cross, the upper bound for the heat transfer rate must be reduced.

If the temperature profiles cross, internal pinching analysis is carried out by introducing the structure that the enthalpies in each stream are expressed as a vector, where the enthalpies in each vector are sorted in increasing value. Therefore, the 0-index for the cold stream enthalpy vector corresponds to the inlet state of the cold stream, and the 0-index for the hot stream vector corresponds to the outlet state of the hot stream.

In the case that there is no phase change for either stream, there will not be any internal pinch points, and the heat transfer rate predicted by Equation (8) is the maximum heat transfer rate in the case of an infinitely large heat exchanger.

In many heat exchangers, one or both of the fluids changes phase, which introduces the possibility of internal pinch points. Based on the analysis predicted by the external pinching heat transfer rate, impossible temperature distributions can be predicted where at some points the hot temperature is colder than the cold stream. Fig. 2(a) shows an example of an impossible configuration predicted by the external pinching analysis. At the internal pinch points, it is known that the cold stream must have a temperature less than the hot stream temperature. For an infinitely large heat exchanger with internal pinching, the temperatures of the two streams will be equal at the limiting internal pinch point, such as can be seen in Fig. 2(b).

To check for internal pinch points, using the maximum heat transfer rate from $\dot{Q}_{max,ext}$, cell division is carried out. At every cell boundary, the temperature for given enthalpy and pressure is evaluated. There are two candidate pinching points described in the following sections that must be considered sequentially. If an internal pinch point is found, the maximum heat transfer rate is reduced and the cell division is carried out using the new prediction of the maximum heat transfer rate.

2.4.1. Hot stream pinch point

If the hot stream has a phase transition from vapor to two-phase, this transition is a possible location for a pinch point. Fig. 3 shows a representation of a heat exchanger with a hot stream phase transition from vapor to two-phase. In this figure, there is

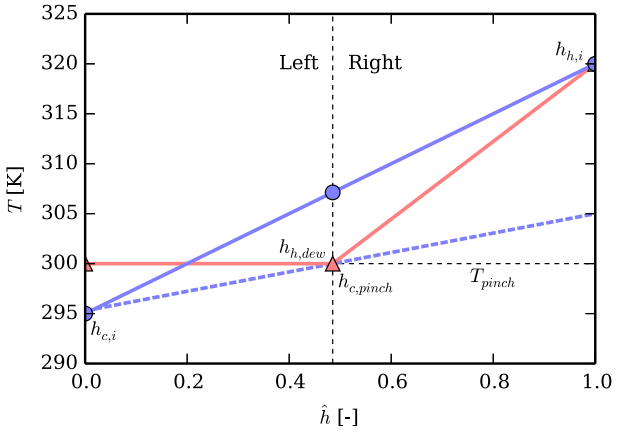

Fig. 3. Hot stream internal pinch point schematic (dashed line shows schematic of profile after pinching analysis is applied).

internal pinching due to the crossing of the temperature profiles. In general, if at the hot fluid phase transition the cold stream temperature is greater than the hot fluid temperature, internal pinching is found.

If pinching is found, the maximum possible heat transfer rate must be decreased to yield the same temperatures for both streams at the pinch point, or $T_{pinch} = T_{h,dew}$. This reduction of the upper bound for the heat transfer is carried out by dividing the heat exchanger into two portions, with the pinch point as the dividing line between the two portions. Using energy balances on each portion, a new, lower prediction for the heat transfer rate can be obtained.

In the right portion of Fig. 3, the inlet enthalpy of the hot stream $h_{h,i}$ is known (it is a model input). The hot stream temperature at the pinch point $T_{h,dew}$ is anchored by the pressure of the hot stream, which allows for the enthalpy of the hot stream at the phase transition $h_{h,dew}$ to be obtained.

The heat transfer in the right-most cell of the heat exchanger is therefore known and can be evaluated from.

$$\dot{Q}_{right} = \dot{m}_h(h_{h,i} - h_{h,dew}). \tag{9}$$

The left portion of the heat exchanger is analyzed by considering that the inlet enthalpy of the cold stream $h_{c,i}$ is known (it is a model input). The enthalpy of the cold stream at the pinch point can be obtained from.

$$h_{c,pinch} = h\left(T_{pinch}, p_{c,i}, \text{Fluid}_c\right) \tag{10}$$

as the pinch point temperature T_{pinch} is known. Thus the total heat transfer in the left portion is.

$$\dot{Q}_{left} = \dot{m}_c\left(h_{c,pinch} - h_{c,i}\right). \tag{11}$$

This analysis assumes that the reduction in heat transfer rate from the internal pinch point analysis will not result in an outlet of the hot stream that is then in the superheated vapor phase.

The new guess for the heat transfer rate in the heat exchanger is then equal to the summation of the heat transfer rates required for the left and right portions, or.

$$\dot{Q}_{max,int} = \dot{Q}_{left} + \dot{Q}_{right}. \tag{12}$$

2.4.2. Cold stream pinch point

Similarly to the hot stream pinch point analysis, when the cold stream has a phase transition from subcooled liquid to two-phase, it is possible that this phase transition can result in internal pinching. If the temperature of the hot stream at this cell boundary is less than the bubble point temperature of the cold stream, the maximum possible heat transfer rate must be decreased to yield the same temperatures for both streams at the pinch point. Fig. 4 shows a schematic of a heat exchanger with crossing temperature profiles, the result of the external pinching analysis. As with the hot stream internal pinching analysis, the goal here is to calculate a new upper bound of the heat transfer rate based on making the temperature profiles coincident at the pinch point temperature.

In the left portion of Fig. 4, the inlet enthalpy of the cold stream $h_{c,i}$ is known (it is a model input). The cold stream temperature at the pinch point $T_{c,bub}$ is anchored by the pressure of the cold stream, which allows for the enthalpy of the hot stream at the phase transition $h_{c,bub}$ to be obtained. The pinch point temperature T_{pinch} is equal to $T_{c,bub}$. The heat transfer in the left portion of the heat exchanger is therefore known and can be evaluated from

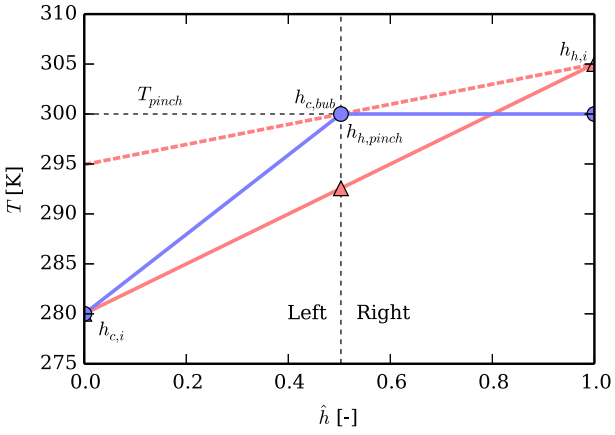

Fig. 4. Cold stream internal pinch point schematic (dashed line shows schematic of profile after pinching analysis is applied).

$$\dot{Q}_{left} = \dot{m}_c(h_{c,bub} - h_{c,i}) \tag{13}$$

The right portion of the heat exchanger is analyzed by considering that the inlet enthalpy of the hot stream $h_{h,i}$ is known (it is a model input). The enthalpy of the hot stream at the pinch point can be obtained from

$$h_{h,pinch} = h\left(T_{pinch}, p_{h,i}, \text{Fluid}_h\right) \tag{14}$$

as the pinch point temperature T_{pinch} is known. Thus the total heat transfer in the right portion is

$$\dot{Q}_{right} = \dot{m}_h\left(h_{h,i} - h_{h,pinch}\right). \tag{15}$$

This analysis assumes that the reduction in heat transfer rate from the internal pinch point analysis will not result in an outlet of the cold stream that is then in the subcooled liquid phase.

The new guess for the heat transfer rate in the heat exchanger is then equal to the summation of the heat transfer rates required for the left and right portions, or

$$\dot{Q}_{max,int} = \dot{Q}_{left} + \dot{Q}_{right}. \tag{16}$$

2.5. Cell division

For a given heat transfer rate $\dot{Q}$, the cell division procedure can be applied. The goal of the cell division procedure is to calculate a vector of enthalpies at the cell boundaries for the hot ($\vec{h}_h$) and cold ($\vec{h}_c$) streams which are sorted in increasing enthalpy, as can be seen in Fig. 5. If there are N cells, there are $N + 1$ cell boundaries. In each cell, energy must be conserved, so the product of $\dot{m}\Delta h$ must be the same for both fluids in each cell which can alternatively be expressed as

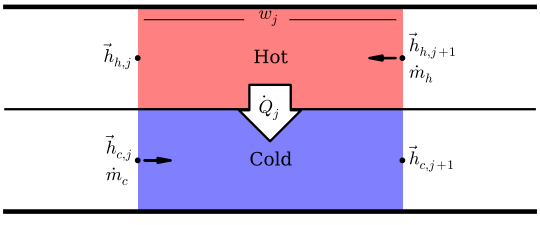

Fig. 5. General schematic for a cell.

$$\dot{m}_h\left(\overrightarrow{h}_{h,j+1} - \overrightarrow{h}_{h,j}\right) = \dot{m}_c\left(\overrightarrow{h}_{c,j+1} - \overrightarrow{h}_{c,j}\right), j = 0, \ldots N-1. \quad (17)$$

In these enthalpy vectors, for a given index j, at least one of $\overrightarrow{h}_{h,j}$ or $\overrightarrow{h}_{c,j}$ must be a phase transition or an inlet or outlet state.

2.5.1. Outlet enthalpies

In the cell division sub-algorithm, the first step is to consider the outlet enthalpies of both streams. The preliminary enthalpy vector for each stream can be calculated from

$$\overrightarrow{h}_h = \left[h_{h,i} - \dot{Q}/\dot{m}_h, h_{h,i}\right] \quad (18)$$

and

$$\overrightarrow{h}_c = \left[h_{c,i}, h_{c,i} + \dot{Q}/\dot{m}_c\right] \quad (19)$$

which are simply the energy balances for each stream over the entire heat exchanger.

2.5.2. Phase transition enthalpies

The next step is to insert the phase transition enthalpies, if they exist, into these enthalpy vectors. For a given pressure, the dew and bubble enthalpies of each stream can be calculated from the saturation pressures of each stream. For instance, $h_{h,bub}$ is the bubble-point enthalpy corresponding to the hot stream inlet pressure $p_{h,i}$.

If a given phase transition enthalpy is within the values from the enthalpy vector given in Equations (18) and (19), it is inserted into the vector, while maintaining both $\overrightarrow{h}_h$ and $\overrightarrow{h}_c$ sorted in increasing value. For instance, if the cold fluid were to evaporate from a two-phase state to a superheated vapor for a given $\dot{Q}$, the cold stream enthalpy vector would be given by.

$$\overrightarrow{h}_c = \left[h_{c,i}, h_{c,dew}, h_{c,i} + \dot{Q}/\dot{m}_c\right]. \quad (20)$$

2.5.3. Complementary phase transition enthalpies

The phase transition enthalpies do not consider all the cell boundaries that may exist in the heat exchanger for a given $\dot{Q}$. Even though the phase transition analysis might not predict any phase transitions of a fluid for a given $\dot{Q}$, it is still possible that a cell division is required to maintain the energy balance in the cells in the heat exchanger.

For instance, in a water-heated-evaporator like that schematically shown in Fig. 2 with two-phase refrigerant inlet, the phase transition enthalpy analysis could predict that there is a phase transition of the cold stream from two-phase to superheated vapor while there are no phase transitions predicted on the water-side. Therefore, a fictitious cell boundary enthalpy needs to be added to the water-side enthalpy vector such that the energy balance from Equation (17) is maintained in each cell. This process is repetitively carried out starting at the left of the heat exchanger (index 0) and working to the right, as for each cell at least three out of four enthalpies are known and the fourth enthalpy can be calculated by the energy balance on the cell.

2.6. Cell analysis

Once the heat exchanger has been divided into cells, it is then possible to determine the fraction of the heat exchanger that each cell requires. The actual heat transfer rate in the cell ($\dot{Q}_j$) is known from.

$$\dot{Q}_j = \dot{m}_c\left(\overrightarrow{h}_{c,j+1} - \overrightarrow{h}_{c,j}\right). \quad (21)$$

The temperatures of each fluid at each cell boundary can be obtained from the values of pressure and enthalpy. Thus it is possible to use the UA-LMTD method to determine the necessary length fraction w_j.

The log-mean-temperature-difference (LMTD) for the cell is defined by

$$\mathrm{LMTD}_j \equiv \frac{\Delta T_{A,j} - \Delta T_{B,j}}{\ln\left(\Delta T_{A,j}/\Delta T_{B,j}\right)} \quad (22)$$

where $\Delta T_{A,j} = \overrightarrow{T}_{h,j+1} - \overrightarrow{T}_{c,j+1}$ and $\Delta T_{B,j} = \overrightarrow{T}_{h,j} - \overrightarrow{T}_{c,j}$. In the case of a cell where both fluids are two-phase pure fluids with no glide during phase change, $\Delta T_{A,j} = \Delta T_{B,j}$ and the LMTD must be replaced with one of $\Delta T_{A,j}$ or $\Delta T_{B,j}$ to avoid division by zero. The LMTD value then allows for the calculation of the required overall thermal conductance in the cell of

$$\mathrm{UA}_{req,j} = \frac{\dot{Q}_j}{\mathrm{LMTD}_j}. \quad (23)$$

The available overall thermal conductance is calculated based on the cell of interest filling the entire heat exchanger, and therefore the areas A_h and A_c refer to the entire hot-side and cold-side areas, respectively. The heat transfer coefficients $\alpha_{h,j}$ and $\alpha_{c,j}$ take the values of the hot- and cold-sides of the heat exchanger in the given cell. Thus the available thermal conductance $\mathrm{UA}_{\mathrm{avail}}$ can be given by

$$\mathrm{UA}_{avail,j} = \frac{1}{\frac{1}{\alpha_{h,j}A_h} + R_{\mathrm{cond}} + \frac{1}{\alpha_{c,j}A_c}} \quad (24)$$

where the thermal conductance resistance based on the A_h area (which can often be neglected) is given by R_{cond}. The mean U factor for the cell can be given by

$$\mathrm{U}_j = \frac{1}{\frac{1}{\alpha_{h,j}} + A_h R_{\mathrm{cond}} + \frac{A_h}{\alpha_{c,j}A_c}} \quad (25)$$

which allows the required area to be calculated from

$$\mathrm{A}_{\mathrm{req},j} = \frac{\mathrm{UA}_{\mathrm{req},j}}{\mathrm{U}_j}. \quad (26)$$

Thus finally the fraction of the heat exchanger required for this cell can be obtained from

$$w_j = \frac{\mathrm{A}_{\mathrm{req},j}}{A_h} \quad (27)$$

2.7. Calculation of heat transfer rate

Once the external and internal pinching analyses have been carried out, it is then known conclusively that the heat transfer rate must be in the open range $(0, \dot{Q}_{max})$ where $\dot{Q}_{max}$ is obtained from the pinching analysis.

Finally, the heat transfer rate $\dot{Q}$ can be obtained from an iterative solution. The residual function to be driven to zero is equal to.

$$r\left(\dot{Q}\right) = 1 - \sum_j w_j \quad (28)$$

which expresses that the sum of the fractions of the total heat exchanger circuit length predicted from each cell of the heat exchanger analysis must be equal to unity when the correct heat transfer rate has been found. At each evaluation of the residual

function, the cell boundaries are recalculated, and the heat transfer analysis is carried out for each cell.

While it is desirable to use a numerical solver like Newton's method or the secant method due to their ease of implementation and/or existing availability in numerical analysis packages, it is often not possible to use these methods due to the shape of the residual function. Newton's method and the secant method are best suited to solving residual functions that have a quasi-linear form over the search domain.

In this case, Newton's method cannot be easily applied to the residual function due to the generally large difference in slope of the residual function at $\dot{Q} = 0$ and $\dot{Q} = \dot{Q}_{max}$. For that reason, a much better choice of numerical solver for this problem is Brent's Method [3]. Brent's method uses a combination of interval bisection and the secant method to yield excellent robustness and computational efficiency. Brent claims that this method is guaranteed to find the solution for a continuous function where the endpoints of the domain bracket the solution. The following Fig. 8 shows an example of a residual function for a water cooled tube-in-tube condenser as described further below. For A = 4 m^2, the solution is very near the elbow in the residual function, causing difficulties for secant-based solvers, while Brent's method can solve this problem with ease.

Brent's method is then used to find the $\dot{Q}$ that enforces the condition $r = 0$ in Equation (28).

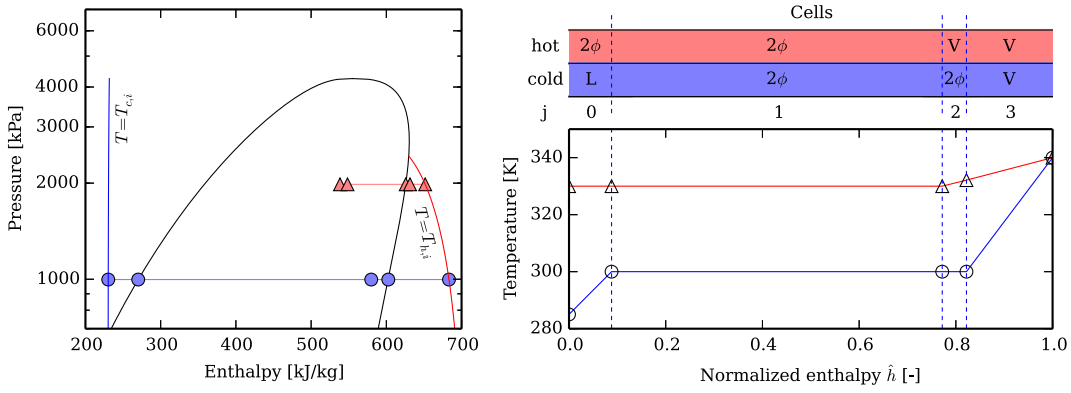

(a) $\dot{m}_h/\dot{m}_c = 0.25$, A = 3 m^2

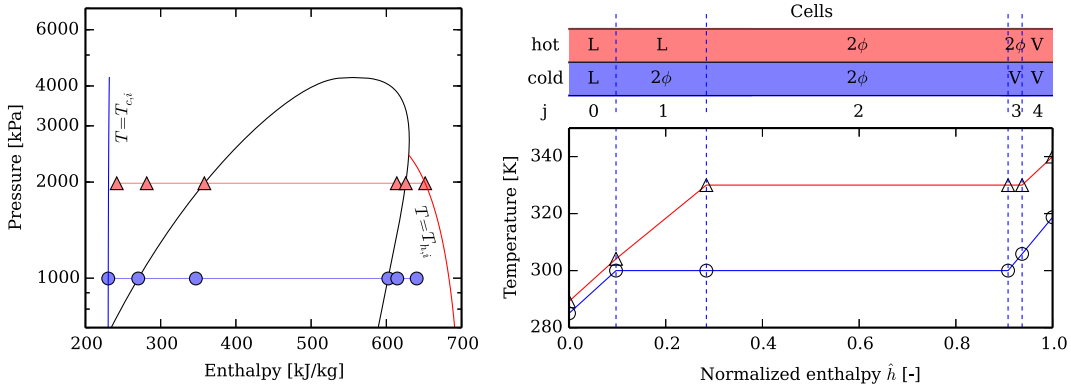

(b) $\dot{m}_h/\dot{m}_c = 1.0$, A = 3 m^2

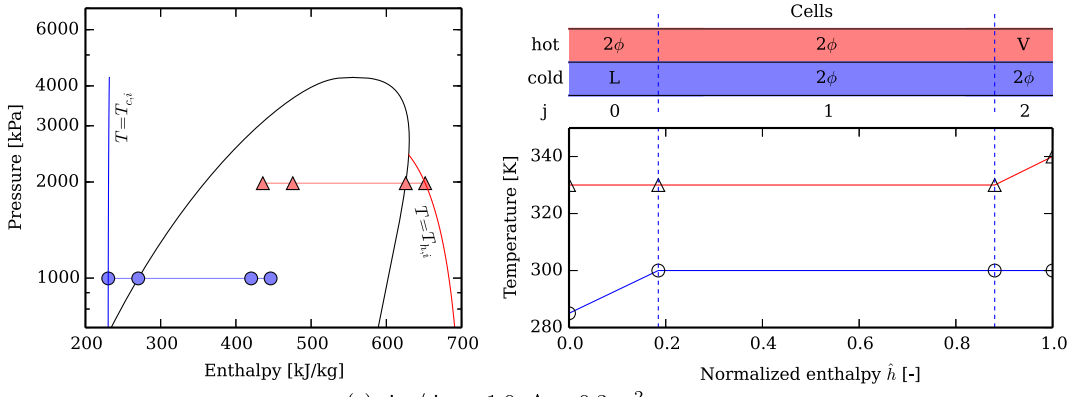

(c) $\dot{m}_h/\dot{m}_c = 1.0$, A = 0.3 m^2

Fig. 6. Full solution analysis for a n-Propane/n-Propane HX ($T_{c,i}$ = 340 K, $T_{h,dew}$ = 330 K, $\dot{m}_h$ = 0.01 kg s^{-1}, $T_{c,i}$ = 285 K, $T_{c,dew}$ = 300 K, L: subcooled liquid, 2ϕ: two-phase, V: superheated vapor).

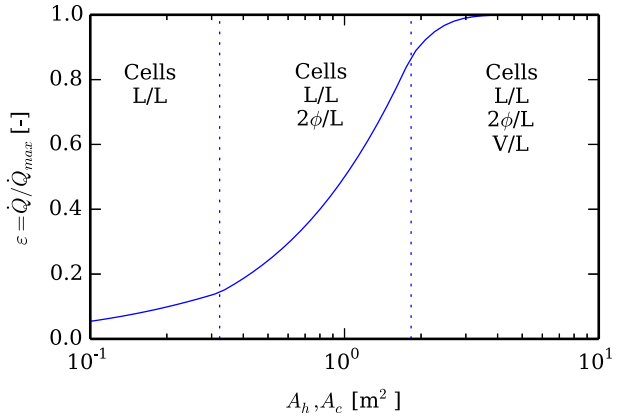

Fig. 7. Propane water-heated evaporator.

2.8. Phase combinations matrix

It can be useful to visualize the large number of phase combinations that are possible in the cells of the heat exchanger. One way of doing this is to consider the phase combination matrix in Table 1, where each cell in the matrix represents a possible cell configuration.

To use this matrix, start at the inlet state for the hot fluid. When there is a phase boundary, the next cell can either be directly to the left or directly down from the current cell. Thus if the hot stream enters as subcooled liquid and the cold stream enters as superheated vapor, the only possible configuration of the heat exchanger is a single cell with subcooled liquid on the hot side and superheated vapor on the cold side. No matter the size of the heat exchanger, it is not possible to reach a phase transition on either side. In practice, the outlet state of both fluids are not known a priori, and it is only after the full solution has been obtained that the phase combinations matrix can be populated. Alternatively the phase combinations matrix can be filled by starting at the inlet state of the cold stream and moving either directly up or directly right at each phase boundary.

As an example, for an air-cooled-condenser, the air (the cold stream) enters as a superheated vapor, and the refrigerant (the hot stream) enters as a superheated vapor. Thus there could be as many as three cells in the heat exchanger, represented by the entries in the matrix in Table 1. If the cold stream enters as subcooled liquid, and the hot stream enters as superheated vapor, there could be as many as five cells. Fig. 6(b)shows an example of a configuration that yields five cells for a n-Propane/n-Propane heat exchanger.

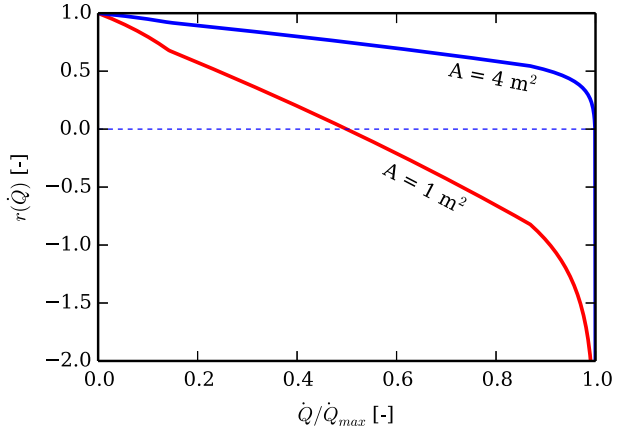

Fig. 8. Residual function from Eqn. (28) for two different areas for the n-Propane evaporator of Table 3.

Table 1
Matrix of all possible phase combinations with possible cells shown for an air-cooled-condenser.

		← Hot ←		
		Liquid	Two-phase	Vapor
Cold ↑	Vapor	X	X	X
	Two-phase			
	Liquid			

2.9. Results

Fig. 6 shows selected results for a n-Propane/n-Propane heat exchanger. The same fluid was selected for both sides in order to be able to readily overlay the pressure and enthalpy state points.

In the first two subfigures, the only difference is the ratio of the mass flow rates of the two streams. When increasing the mass flow rate ratio from 0.25 to 1.0, the pinch point moves from the outlet of the cold stream to the internal pinch point between the bubble point of the cold stream and the hot stream. This is the expected behavior; changing the ratios of mass flow rates will often change the limiting thermodynamic states. This is one of the complicating factors associated with modeling of heat exchangers with phase change. For heat exchangers without phase change, the pinch point (and the maximum heat transfer rate) can be readily defined. For heat exchangers with the possibility of phase change, it is more challenging to define the maximum possible heat transfer rate.

Fig. 6(b) shows a heat exchanger with five cells, the maximum possible number. In this heat exchanger it is possible to see a wide range of model features, including internal pinching and two-phase and single-phase complementary phase boundaries. The phase combination matrix for Fig. 6(b) is shown in Table 2.

In Fig. 6(c), the area from Fig. 6(b) is reduced. As a consequence, the rate of heat transfer decreases, and the closest approach temperature is that between the saturation temperature corresponding to the inlet pressures of both streams.

3. Example case

This model can be exercised to consider a few different practical cases in order to demonstrate its use. In more detailed analysis, the heat transfer coefficients are calculated based on correlations, while in this case for illustrative purposes the heat transfer coefficients are constant and specified based on the phase of the fluid in the cell:

- Superheated vapor: $\alpha = 100$ W m^{-2} K^{-1}
- Two-phase: $\alpha = 2000$ W m^{-2} K^{-1}
- Subcooled liquid: $\alpha = 100$ W m^{-2} K^{-1}

Table 2
Cell phase combination matrix for Fig. 6(b).

		← Hot ←		
		Liquid	Two-phase	Vapor
Cold ↑	Vapor		X	X
	Two-Phase	X	X	
	Liquid	X		

3.1. Single-phase-heated evaporator

In this section a n-Propane evaporator is further analyzed to demonstrate the application of this algorithm. The evaporator is as described in Table 3 with a n-Propane subcooled liquid inlet that is fed with warmer subcooled water in order to evaporate the n-Propane. Table 3 does not provide the areas A_h or A_c as they are considered here to be adjustable parameters.

The adjustment of the area of the heat exchanger for the given mass flow rates and inlet states can yield very different behavior of the heat exchanger, and has a profound impact on the effectiveness of the heat exchanger. For heat exchangers that do not have any interior phase boundaries, there are analytic definitions for the effectiveness of the heat exchanger that can be found in conventional heat transfer literature [5]. In the case of the generalized heat exchanger treatment covered here with multiple phase boundaries, the effectiveness can be defined in a similar way. But unlike the simple heat exchangers, the maximum heat transfer rate cannot be obtained in a simple way because it must take into account both internal and external pinching.

Fig. 7 shows the impact on the effectiveness of the heat exchanger as the area of the heat exchanger is increased. Both the hot stream and the cold stream are imposed to have the same area A, or $A = A_h = A_c$. As the area of the heat exchanger is increased, the effectiveness of the heat exchanger increases monotonically. In the limit that the area of the heat exchanger goes to zero, there is no heat transfer because the overall thermal conductance of the heat exchanger also goes to zero. For relatively small heat exchangers (small area), there is only one cell in the heat exchanger, a subcooled liquid n-Propane/subcooled liquid water cell. As the area of the heat exchanger is increased, a two-phase n-Propane/subcooled liquid water cell is added at an area of approximately 0.31 m^2. Adding further area to the heat exchanger yields an additional superheated vapor cell at an area of 1.75 m^2. Referring back to Table 1, the inlet state to the heat exchanger is in the bottom left corner of the matrix, and the cells are added in the left-most column.

Considering now two particular heat exchanger areas, further features of the algorithm can be explored. Fig. 8 shows the residual functions for a range of heat transfer rates for two different areas of 1 m^2 and 4 m^2. The goal of the algorithm is to obtain the value $\dot{Q}$ corresponding to $r(\dot{Q}) = 0$. Thus from the description associated with Fig. 7, it can be noted that for an area of 1 m^2, there are two cells, one with subcooled n-Propane and one with two-phase n-Propane, with subcooled water in both cells. For an area of 4 m^2, there are three cells. Importantly, there is a significant difference in the shape of the residual function between the two different areas of 1 m^2 and 4 m^2. For the area of 1 m^2, the residual function is nearly linear with the heat transfer rate around the solution, and thus Brent's method solver will converge rapidly to the solution. Conversely, the residual function for an area of 4 m^2 is a much more challenging residual function to solve numerically because the solution lies in the vicinity of a sharp change in the derivative of the residual function.

Table 3
Fixed values for the propane evaporator analysis.

Parameter	Value
Fluid_h	Water
$T_{h,i}$	330 K
$p_{h,i}$	101,325 Pa
$\dot{m}_h$	0.01 kg s^{-1}
Fluid_c	*n*-Propane
$T_{c,i}$	275 K
$T_{c,dew}$ (and $T_{c,bub}$)	300 K
$\dot{m}_c$	0.1 kg s^{-1}
R_{cond}	0

Fig. 9 shows the residual function history of Brent's method as it approaches the solution. From these results it can seen that there is a strong difference in the rate of convergence of Brent's method for the two different areas, as could be predicted by considering the shape of the residual functions. For an area of 1 m^2, Brent's method requires a few steps to approach the solution, after which it converges rapidly to the desired solution. On the other hand, for an area of 4 m^2, Brent's method requires quite a few midpoint iteration steps at the beginning to approach the solution, after which it too rapidly approaches the solution. For a residual function tolerance, Brent's method takes approximately 10 more steps for an area of 4 m^2 than for an area of 1 m^2.

3.2. Computational efficiency

One of the primary motivations for the use of moving boundary models is their superior computational efficiency as compared to finite difference or finite volume models. While the accuracy of moving boundary models tends to be somewhat lower than finite difference or finite volume models, the loss in accuracy is not very severe.

For a range of areas between 1 and 7 m^2 for the n-Propane evaporator of Table 3, the run time for one execution of the entire model (pinching analysis + solution) is 24.6 ms, averaged out over 20,000 runs. These results were obtained on a 64-bit 2.7 GHz i7-2620M Intel processor with 8 GB of RAM, with 32-bit Python 2.7.2 and CoolProp 4.2.

In the simulation code, nearly all the computational effort is spent evaluating thermodynamic properties. The challenge here is that the primary set of thermodynamic inputs used in this model are pressure and enthalpy. This set of thermodynamic variables is challenging because the equations of state are all formulated with temperature and density as the independent variables. Furthermore, the use of water as a working fluid in this case causes further challenges because the equation of state for ordinary water [14] is the most computationally expensive equation of state in the literature. The equation of state for *n*-Propane [8] is closer to the median computational complexity.

In the thermodynamic code from CoolProp, a Newton–Raphson two-dimensional solver is used to carry out the transformation $p,h \rightarrow T,\rho$ after appropriate preconditioning. The computational efficiency of the calculation of the thermodynamic state given pressure and enthalpy can be greatly improved through the use of interpolation methods like that of the Tabular Taylor Series Expansion (TTSE) method [9]. This method has been implemented in CoolProp, and when TTSE is used to carry out the transformation

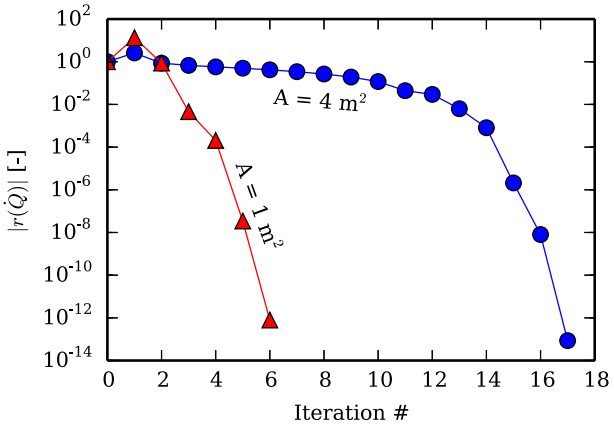

Fig. 9. Absolute value of residual function at each step of the iteration for two different areas.

$p,h \rightarrow T,\rho$, the computational speedup is significant. For the same set of 20,000 runs, the elapsed time for one run with TTSE enabled is 2.46 ms, or a speedup ratio of 10 times through the use of TTSE. The results for the predicted heat transfer rate differ by less than 0.001% between the use of the full equation of state and the TTSE method.

4. Conclusions

In this paper a robust algorithm has been presented that can be used to determine the thermal duty for heat exchangers that have inlet states that are two-phase or single-phase. This algorithm is provided in open-source in the electronic annex of this paper to facilitate its practical use for the reader. This algorithm uses pinch point analysis to calculate the bounds for the thermal duty and then the very robust Brent's method to yield the solution. This algorithm is computationally efficient, taking on the order of one millisecond to complete one entire run when the Tabular Taylor Series Expansion method is employed. The use of Brent's method to solve the residual equation guarantees that the solution can be found. Future work could allow for pressure drop in the cells of the heat exchanger, as well as the investigation of non-pure-counterflow configurations.

Acknowledgements

The authors would like to acknowledge the contributions of Brandon Woodland of Purdue University; he was instrumental in developing the first version of the model.

Appendix A. Supplementary data

Supplementary data related to this article can be found at http://dx.doi.org/10.1016/j.applthermaleng.2014.12.

References

[1] I.H. Bell, J. Wronski, S. Quoilin, V. Lemort, Pure and pseudo-pure fluid thermophysical property evaluation and the open-source thermophysical property library CoolProp, Ind. Eng. Chem. Res. 53 (6) (2014) 2498–2508. URL: http://pubs.acs.org/doi/abs/10.1021/ie4033999.
[2] S. Bendapudi, J. Braun, E.A. Groll, A comparison of moving-boundary and finite-volume formulations for transients in centrifugal chillers, Int. J. Refrig. 31 (2008) 1437–1452.
[3] R. Brent, Algorithms for Minimization Without Derivatives, Prentice-Hall, 1973. Ch. 4.
[4] G.-L. Ding, Recent developments in simulation techniques for vapour-compression refrigeration systems, Int. J. Refrig. 30 (2007) 1119–1133.
[5] F.P. Incropera, D.P. Dewitt, Fundamentals of Heat and Mass Transfer, fifth ed., Wiley, 2002.
[6] S.G. Kandlikar, R.K. Shah, Multipass plate heat exchangers-effectiveness-NTU. Results and guidelines for selecting pass arrangements, ASME J. Heat Transf. 111 (1989) 300–313.
[7] E. Lemmon, M. Huber, M. McLinden, NIST Standard Reference Database 23: Reference Fluid Thermodynamic and Transport Properties-REFPROP, Version 9.1, 2013.
[8] E.W. Lemmon, M.O. McLinden, W. Wagner, Thermodynamic properties of propane. III. A reference equation of state for temperatures from the melting line to 650 K and pressures up to 1000 MPa, J. Chem. Eng. Data 54 (2009) 3141–3180.
[9] K. Miyagawa, P. Hill, Rapid and accurate calculation of water and steam properties using the tabular Taylor series expansion method, J. Eng. Gas Turb. Power 123 (2001) 707–712.
[10] H. Qiao, V. Aute, H. Lee, K. Saleh, R. Radermacher, A new model for plate heat exchangers with generalized flow configurations and phase change, Int. J. Refrig. 36 (2013) 622–632.
[11] S. Quoilin, Sustainable Energy Conversion Through the Use of Organic Rankine Cycles for Waste Heat Recovery and Solar Applications (Ph.D. thesis), University of Lige, 2011.
[12] C. Ribeiro Jr., M.C. Andrade, An algorithm for steady-state simulation of plate heat exchangers, J. Food Eng. 53 (2002) 59–66.
[13] A. Settari, J. Venart, Approximate method for the solution to the equations for parallel and mixed-flow multi-channel heat exchangers, Int. J. Heat Mass Transf. 15 (1972) 819–829.
[14] W. Wagner, A. Pruss, The IAPWS formulation 1995 for the thermodynamic properties of ordinary water substance for general and scientific use, J. Phys. Chem. Ref. Data 31 (2002) 387–535.
[15] J. Wolf, General solution of the equations of parallel-flow multichannel heat exchangers, Int. J. Heat Mass Transf. 7 (1964) 901–919.
[16] Y. Yohanis, O. Popel, S. Frid, A simplified method of calculating heat flow through a two-phase heat exchanger, Appl. Therm. Eng. 25 (2005) 2321–2329.
[17] T. Zaleski, K. Klepacka, Approximate method of solving equations for plate heat exchangers, Int. J. Heat Mass Transf. 35 (1992) 1125–1130.